Spin response and collective modes in simple metal dichalcogenides

Dibya Kanti Mukherjee,[1] Arijit Kundu,[2] and H. A. Fertig[3]

[1]*Harish-Chandra Research Institute, HBNI, Chhatnag Road, Jhunsi, Allahabad 211 019, India*
[2]*Department of Physics, Indian Institute of Technology Kanpur, Kanpur 208016, India*
[3]*Department of Physics, Indiana University, Bloomington, Indiana 47405, USA*

Transition-metal dichalcogenide monolayers are interesting materials in part because of their strong spin-orbit coupling. This leads to intrinsic spin splitting of opposite signs in opposite valleys, so the valleys are intrinsically spin polarized when hole doped. We study spin response in a simple model of these materials, with an eye to identifying sharp collective modes (i.e., spin waves) that are more commonly characteristic of ferromagnets. We demonstrate that such modes exist for arbitrarily weak repulsive interactions, even when they are too weak to induce spontaneous ferromagnetism. The behavior of the spin response is explored for a range of hole dopings and interaction strengths.

I. INTRODUCTION

Two-dimensional materials based on honeycomb lattices have become the subject of intense investigation in the past few years due to their interesting band structure and associated topological properties. The low-energy dynamics of such systems are typically dominated by states near the K and K' points in the Brillouin zone. The paradigm of this is realized in graphene, a pure carbon honeycomb lattice, which hosts a gapless spectrum with Dirac points at these locations [1] due to a combination of inversion and time-reversal symmetry, as well as the very weak spin-orbit coupling (SOC) typical of light elements. More recently, transition-metal dichalcogenide (TMD) monolayers, where a transition metal M (e.g., Mo or W) resides on one sublattice and a dimer of chalcogen X atoms (e.g., S, Se) resides on the other, have emerged as important materials in this class [2,3]. These systems are gapped at the K and $K' = -K$ points, and the strong SOC associated with M atoms leads to very interesting spin-valley coupling near these points [4,5]. In particular, one finds spin-up and -down components of the valence band well separated in energy, with their ordering interchanged for the two valleys. This allows for an effective valley polarization to be induced when the system spin polarizes via pumping with circularly polarized light [6–8]. The coupling of spin and valley in this way has been dramatically demonstrated via the observation of a valley Hall effect in this circumstance [9].

The locking of spin and valley degrees of freedom in TMD monolayers is a unique feature of these materials. When hole doped, it leads to a nonzero expectation value of $\sigma_z \tau_z$, where σ_z is a Pauli matrix for spin and τ_z is the analogous operator for the valley index. This occurs without any interaction present in the Hamiltonian yet is reminiscent of ferromagnetic ordering, albeit without time-reversal symmetry breaking since this reverses both the spin and valley. Recently, it was argued that for strong enough interactions, TMD systems develop a spontaneous imbalance of spin and valley populations [10,11], which leads to actual ferromagnetic spin order

in the ground state. It thus becomes interesting to consider how one might probe and distinguish these orderings. One possible strategy is to investigate the spin response of the system, both to search for sharp collective modes that are a hallmark of ferromagnets and to understand broader features of the response that demonstrate the ordering present in these materials. This is the subject of our study.

We focus on the basic qualitative physics of this system by employing a simple two-band model for MX_2 compounds [4] with a short-range repulsive interaction and compute the spin response using the time-dependent Hartree-Fock approximation [12]. For concreteness quantitative results are computed using parameters appropriate for MoS_2, and we examine results for several representative hole dopings and interaction strengths. A typical result is illustrated in Fig. 1 for a system with low hole doping, such that only a single spin species of the valence band is partially unoccupied in each of the valleys.

For small wave vectors q, a sharp collective mode is visible below a continuum of particle-hole spin-flip excitations which are present even in the absence of interactions (although the frequency interval where they reside is renormalized by them). An interesting feature of the collective mode is that, for low hole doping, it is present for arbitrarily weak interaction strength, even if the system is not spin ferromagnetic. Its presence may be understood as arising from the effective $\sigma_z \tau_z$ polarization that is induced when the system is hole doped. Interestingly, this is a direct analog of Silin-Leggett modes [13,14] that appear when fermions become spin polarized by an external magnetic field. In that system, the noninteracting Hamiltonian induces a spin polarization in the ground state which is not present spontaneously. Nevertheless, the combination of different Fermi surfaces for different spins, together with exchange interactions which energetically favor ferromagnetism locally, leads to sharp, collective excited states of low energy. These modes have been detected in spin-polarized ^{3}He [15].

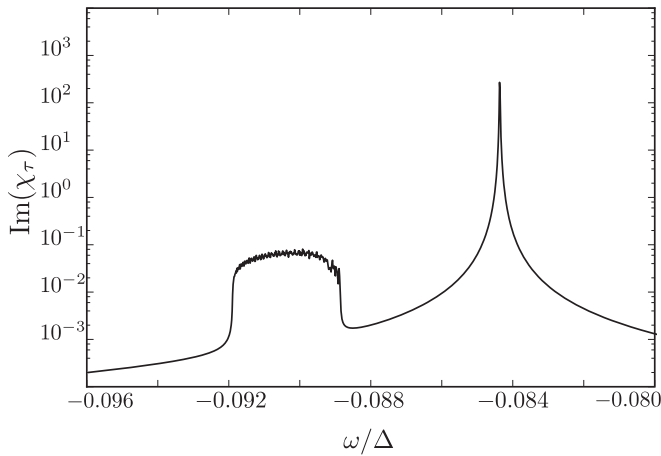In the TMD system, an analogous sharp response appears when the system absorbs angular momentum, typically from

FIG. 1. Absorptive part of the spin response function Im $\chi_\tau(\mathbf{q}, \omega)$ for $\mathbf{q} = 0$, chemical potential $\mu_0 = -0.49\Delta$, and $U_0 = 0.2$ eV, with $\tau = +1$. Model parameters for band structure are given in Table I. A sharp collective mode near $\omega \approx -0.0845\Delta$ is prominent above a particle-hole continuum in the interval $-0.092 \lesssim \omega/\Delta \lesssim -0.087$, where $\Delta = 1.66$ eV.

a photon, and is dominated by excitations around one of the two valleys. The spin response from the other valley is negligible around these frequencies but can be seen at negative frequencies, which is equivalent to absorption of photons with the opposite helicity. This effect is well known in the context of undoped TMD systems [6–8] where the particle-hole excitations involve electrons excited from the valence to the conduction band. In the present situation one finds this behavior from excitations within the valence band, from occupied spin states to unoccupied ones available due to the doping of opposing spin. The resulting sharp modes are much lower in energy than comparable exciton modes of an undoped system [16–19].

True ferromagnetism in this system has been argued to arise when interactions are sufficiently strong that unequal populations of the two valleys become energetically favorable [10,11], and for a hole-doped, short-range interaction model, it occurs as a first-order transition at a critical interaction strength U_c [11]. Within our model this results in an effective shift of the bands relative to one another, so that a system sufficiently clean and cold to allow observation of resonances associated with collective spin modes would present them at different frequencies for different helicities.

At higher dopings the valence bands will support two Fermi surfaces in each valley, indicating that they contain holes of both spins. Because of the opening of the second Fermi surface the system now supports gapless spin-flip excitations, albeit at finite wave vector. Regions in frequency and wave vector where these exist are illustrated in Fig. 2, along with the spin-wave dispersion for these parameters. Observation of such a continuum of gapless modes would allow a direct demonstration of the spin-split Fermi surfaces in this system. In practice, because these modes appear above wave vectors of order $q \lesssim 1/a$, with a being the lattice constant, their presence may be difficult to observe by direct electromagnetic absorption because of momentum conservation.
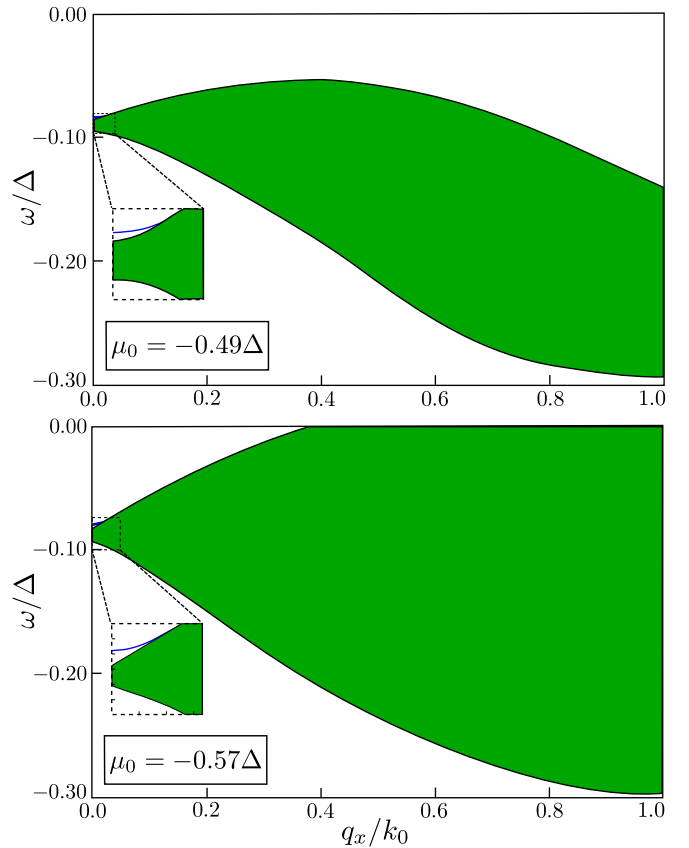

FIG. 2. The top panel, for $\mu_0 = -0.49\Delta$, in which there is only a single Fermi surface in the valley (demonstrated in Fig. 3), has a continuum of particle-hole excitations (shown in green) below some minimum frequency. The bottom panel has $\mu_0 = -0.57\Delta$, for which there are two Fermi surfaces in the valley, giving rise to the continuum modes with vanishingly small energies for $q_x > 0.4k_0$, with $k_0 = \Delta/2ta$. For both panels, $U_0 = 0.2$eV and $\tau = +1$. Other parameters are listed in Table I. Blue lines illustrate the collective spin-wave mode dispersion.

In real systems, disorder relaxes this constraint and may make their detection feasible [20].

Our analysis also shows that the system, in principle, supports a *second* collective spin-wave mode, one associated with interorbital spin flips. This mode exists extremely close to the edge of the continuum of particle-hole spin excitations and in practice might be difficult to discern in the spin response function. Its presence would presumably be more easily detected in response functions that combine interorbital excitations with spin flips.

This paper is organized as follows. In Sec. II we describe both the single-particle Hamiltonian and the interaction model we adopt for this system. Section III describes a static Hartree-Fock analysis of the system, demonstrating that the effective single-particle Hamiltonian is rather similar to the noninteracting one, with renormalized parameters. In Sec. IV we carry out a time-dependent Hartree-Fock analysis of the spin response function and show how one can identify poles that signal allowed spin-flip excitations of the system. In Sec. V we carry out an analytic analysis of the equations generated in the previous section appropriate for low hole

TABLE I. Values of various parameters for MoS$_2$ from Ref. [4].

a	t	Δ	λ
3.190 Å	1.059 eV	1.66 eV	0.075 eV

doping. Section VI provides results one finds from numerical solutions for the spin response functions. We conclude with a summary in Sec. VII.

II. MODEL OF THE SYSTEM

Our starting point is a simple two-band Hamiltonian for a monolayer MX_2, such as MoS$_2$, developed through several numerical, symmetry-based analyses [4] which capture the electronic properties near the K, $-K$ valleys. In the absence of interactions this has the form

$$H_0^\tau(\mathbf{k}) = \begin{bmatrix} \Delta/2 & at(\tau k_x - ik_y) \\ at(\tau k_x + ik_y) & -\Delta/2 + s\tau\lambda \end{bmatrix}, \quad (1)$$

which is written in the basis $|\psi_c^\tau\rangle = |d_{z^2}\rangle$ and $|\psi_v^\tau\rangle = \frac{1}{\sqrt{2}}(|d_{x^2-y^2}\rangle + i\tau|d_{xy}\rangle)$, where $\tau = \pm$ is the valley index, t is the hopping matrix element, and d_{z^2}, $d_{x^2-y^2}$, d_{xy} are orbitals of the M atoms. (Here and throughout this paper we take $\hbar = 1$.) Spin is a good quantum number, denoted by $s = 1$ for ↑ and $s = -1$ for ↓. The strength of spin-orbit coupling is encoded in the parameter λ. In the ground state of this Hamiltonian, states up to the chemical potential μ_0, which is tunable, in principle, via gating, are filled. Estimates [4] for the parameters relevant to MoS$_2$ are listed in Table I.

The energy eigenstates of the full Hamiltonian with momentum $\mathbf{k}$ and spin s will be denoted by $\phi_{l,s}(\mathbf{k})$, with $l = \{\tau, \alpha\}$ ($\alpha = \pm$ for conduction and valence bands, respectively), and have the form

$$\phi_{l,s}(\mathbf{k}) = \frac{1}{\sqrt{2}} \begin{pmatrix} \tau e^{-i\tau\phi}\sqrt{1 + \frac{\alpha m_{s\tau}}{\sqrt{m_{s\tau}^2 + a^2t^2k^2}}} \\ \alpha\sqrt{1 - \frac{\alpha m_{s\tau}}{\sqrt{m_{s\tau}^2 + a^2t^2k^2}}} \end{pmatrix}, \quad (2)$$

with corresponding eigenvalues

$$\epsilon_{l,s}^\alpha(\mathbf{k}) = \frac{\tau s\lambda}{2} + \alpha\sqrt{m_{s\tau}^2 + (atk)^2}, \quad (3)$$

where $m_{s\tau} = \frac{\Delta - \tau s\lambda}{2}$ and $k = \sqrt{k_x^2 + k_y^2}$. The bands near the K ($\tau = 1$) valley, shown in Fig. 3, illustrate the distinct spin structure of the system. The valence and conduction bands are separated by a relatively large gap $E_g = (\Delta - \lambda)$ at $k = 0$, whereas the two spin valence bands are further separated by a smaller gap of magnitude $E_\lambda = 2\lambda$. This gap between the spin-split valence bands remains almost constant for a range of k until $akt \gg \Delta$. Note that the two conduction bands of the model are nearly degenerate. The K and $-K$ valleys of the system are related by time reversal, so that the spins of the two bands are reversed in going from one to the other.

To write down an effective interaction, it is convenient to define field operators of spin s projected into the set of states defined in our model,

$$\Psi_s(\mathbf{r}) = \frac{1}{\sqrt{L_x L_y}} \sum_{\mathbf{k},l} e^{i(\mathbf{k}+\mathbf{K}_{\tau_l})\cdot\mathbf{r}} \phi_{l,s}(\mathbf{k}) c_{l,s}(\mathbf{k}), \quad (4)$$
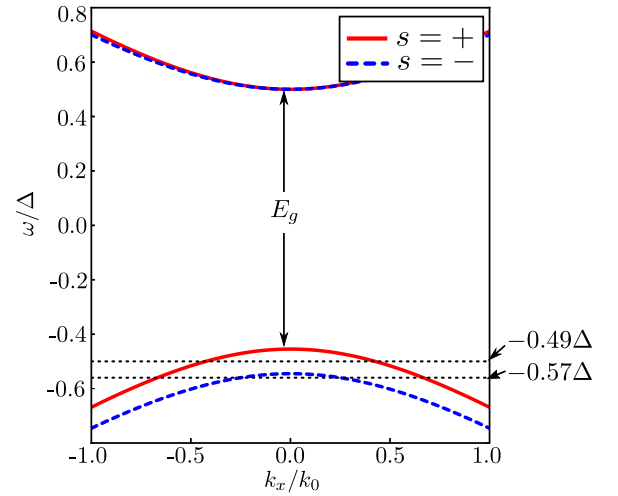

FIG. 3. The band dispersion of Hamiltonian (1) showing a direct band gap E_g between the valence and conduction bands and the separation of spin-polarized bands in the conduction band. Positions for two μ_0 are marked in the right margin. $k_0 = \Delta/2ta$ is the scale of momentum. The parameters used are listed in Table 1, and $\tau = +1$.

where $c_{l,s}(\mathbf{k})$ is the annihilation operator for the l, s state at momentum $\mathbf{k}$ relative to the valley minima and maxima at $\mathbf{K}_{\tau_l} = \tau_l\mathbf{K}$, with the sign determined by the τ index implicit in l, and $L_x L_y$ is the area of the system. A repulsive interaction among the band electrons can then be represented in the form

$$H_{\text{int}} = \frac{1}{2} \sum_{s,s'} \int d^2\mathbf{r}\, d^2\mathbf{r}'\, V(\mathbf{r} - \mathbf{r}') :$$
$$\Psi_s^\dagger(\mathbf{r})\Psi_s(\mathbf{r})\Psi_{s'}^\dagger(\mathbf{r}')\Psi_{s'}(\mathbf{r}') :, \quad (5)$$

where V represents a finite-range repulsive interaction. Physically, this arises from Coulomb interactions among the band electrons; the finite range can be provided by a screening gate or by carriers in the layer itself (although we will not treat the screening dynamically in what follows). We assume the screening length is large on the scale of the lattice constant, so that intervalley contributions to the density $\Psi_s^\dagger(\mathbf{r})\Psi_s(\mathbf{r})$ oscillate rapidly and can be ignored when integrated over $\mathbf{r}$. This leads to the replacement

$$H_{\text{int}} \to \frac{1}{2} \sum_{s,s'} \sum_{\tau,\tau'} \int d^2\mathbf{r}\, d^2\mathbf{r}'\, V(\mathbf{r} - \mathbf{r}') :$$
$$\Psi_{s\tau}^\dagger(\mathbf{r})\Psi_{s\tau}(\mathbf{r})\Psi_{s'\tau'}^\dagger(\mathbf{r}')\Psi_{s'\tau'}(\mathbf{r}') :, \quad (6)$$

with

$$\Psi_{s\tau}(\mathbf{r}) = \frac{1}{\sqrt{L_x L_y}} \sum_{\mathbf{k},l} e^{i\mathbf{k}\cdot\mathbf{r}} \phi_{l,s}(\mathbf{k}) c_{l,s}(\mathbf{k})\delta_{\tau,\tau_l}, \quad (7)$$

where τ_l is the valley content of the composite l index. At this point we can make the approximation $V(\mathbf{r} - \mathbf{r}') = 2U_0\delta^2(\mathbf{r} - \mathbf{r}')$ and arrive at an interaction with the form

$$H_{\text{int}} = U \sum_{\{l_i \mathbf{k}_i \mathbf{q}\}} \sum_{s,s'} \phi_{l_1 s}^\dagger(\mathbf{k}_1)\phi_{l_2 s'}^\dagger(\mathbf{k}_2)\phi_{l_3 s'}(\mathbf{k}_2 + \mathbf{q}')$$
$$\times \phi_{l_4 s}(\mathbf{k}_1 - \mathbf{q}')\delta_{\tau_{l_1},\tau_{l_4}}\delta_{\tau_{l_2},\tau_{l_3}} c_{l_1 s}^\dagger(\mathbf{k}_1)c_{l_2 s'}^\dagger(\mathbf{k}_2)$$
$$\times c_{l_3 s'}(\mathbf{k}_2 + \mathbf{q}')c_{l_4 s}(\mathbf{k}_1 - \mathbf{q}'), \quad (8)$$

where $U = \frac{U_0}{L_x L_y}$. This is the interaction Hamiltonian that we use in the Hartree-Fock analyses that follow.

III. HARTREE-FOCK APPROXIMATION

In order to carry out an analysis of the spin response in this system within the time-dependent Hartree-Fock approximation, it is first necessary to find the density matrix of the system within the static Hartree-Fock (HF) approximation. This has the form

$$\langle c_{ls}^\dagger(\mathbf{k}) c_{l's'}(\mathbf{k}') \rangle = n_{ls}(\mathbf{k}) \delta_{ll'} \delta_{ss'} \delta_{\mathbf{k},\mathbf{k}'}. \quad (9)$$

Note in writing this, we have assumed that neither interband nor intervalley coherence has formed in the system spontaneously. Performing a HF decomposition on Eq. (8) gives a potential for an effective single-body Hamiltonian,

$$H_{\text{int}}^{\text{HF}} = -2U \sum_{ll',ss',\mathbf{k}} \delta_{ss'} \sum_{a,b=A/B} c_{ls}^\dagger \phi_{ls}^{a*}(\mathbf{k})$$

$$\times \left(\sum_{l''} \phi_{ls}^a(\mathbf{k}) n_{l''s}(\mathbf{k}) \phi_{l''s}^{b*}(\mathbf{k}) \right) \phi_{l's}^b(\mathbf{k}) c_{l's}, \quad (10)$$

where, for notational simplicity, we have used the a, b indices to denote the orbital degree of freedom [$A \equiv |d_{z^2}\rangle$ and $B \equiv \frac{1}{\sqrt{2}}(|d_{x^2-y^2}\rangle + i\tau |d_{xy}\rangle)$]. The full HF Hamiltonian for electrons with wave vector $\mathbf{k}$ then becomes

$$H_{ls,l's}^{0,\text{HF}}(\mathbf{k}) = H_{ls,l's}^0(\mathbf{k}) - 2U \sum_{ab} \phi_{ls}^{a*}(\mathbf{k}) n_s^{ab} \phi_{l's}^b(\mathbf{k}), \quad (11)$$

with $n_{s_l}^{ab} = \sum_{\mathbf{k}l} \phi_{ls}^a(\mathbf{k}) n_{ls}(\mathbf{k}) \phi_{ls}^{b*}(\mathbf{k})$. The quantities n_{ls} need to be determined self-consistently. Note in writing $H_{ls,l's}^{0,\text{HF}}(\mathbf{k})$, we have dropped a term proportional to the total fermion number which is a constant. In the orbital basis (l, l') one may write

$$H^{0,\text{HF}}(\mathbf{k}) = \begin{bmatrix} \tilde{m}_{s\tau} & at\tau k e^{-i\tau\phi} \\ at\tau k e^{i\tau\phi} & -\tilde{m}_{s\tau} \end{bmatrix}$$

$$+ \tau s\lambda/2 - U(n_{s\tau}^{AA} + n_{s\tau}^{BB}), \quad (12)$$

with renormalized mass $\tilde{m}_{s\tau} = \frac{\Delta - \tau s\lambda}{2} - U(n_{s\tau}^{AA} - n_{s\tau}^{BB})$. For a fixed density (obtained by fixing μ_0), the value of $\tilde{m}_{\tau s}$

is found numerically using the requirement that the values $n_{ls}(k)$ used to generate Eq. (12) yield wave functions that produce the very same values; that is, the density matrix used to generate the HF Hamiltonian is the same as what one finds from its eigenvectors and eigenvalues. In the present case, the wave functions have a functional form that is the same as that of the free wave functions, Eq. (2), with modified parameters:

$$\phi_{l,s}(\mathbf{k}) = \frac{1}{\sqrt{2}} \begin{pmatrix} \tau e^{-i\tau\phi} \sqrt{1 + \frac{\alpha \tilde{m}_{s\tau}}{\sqrt{\tilde{m}_{s\tau}^2 + a^2 t^2 k^2}}} \\ \alpha \sqrt{1 - \frac{\alpha \tilde{m}_{s\tau}}{\sqrt{\tilde{m}_{s\tau}^2 + a^2 t^2 k^2}}} \end{pmatrix}. \quad (13)$$

The energy eigenvalues then become

$$\tilde{\epsilon}_{l,s}(\mathbf{k}) = \frac{\tau s\lambda}{2} + \alpha \sqrt{\tilde{m}_{s\tau}^2 + (atk)^2} - U(n_{\tau s}^{AA} + n_{\tau s}^{BB}), \quad (14)$$

which is similar but not identical to the noninteracting energy eigenvalues, Eq. (3). Here, in analogy with the previous section, the index $l = \{\tau, \alpha\}$ implicitly contains the valley index τ as well as the conduction/valence band index $\alpha = \pm 1$. In the remainder of this paper, we will use these as the basis states for our analysis.

IV. TIME-DEPENDENT HARTREE-FOCK APPROXIMATION

Our focus in this study is the spin-spin response function

$$\chi_\tau(\mathbf{r} - \mathbf{r}', t) = -i\Theta(t) \langle [\rho_\tau^{+-}(\mathbf{r}, t), \rho_\tau^{-+}(\mathbf{r}', 0)] \rangle, \quad (15)$$

with $\rho_\tau^{\sigma\sigma'}(\mathbf{r}, t) = \Psi_{\sigma\tau}^{\text{HF}\dagger}(\mathbf{r}, t) \Psi_{\sigma'\tau}^{\text{HF}}(\mathbf{r}, t)$, with field operators

$$\Psi_{s\tau}^{\text{HF}}(\mathbf{r}) = \frac{1}{\sqrt{L_x L_y}} \sum_{\mathbf{k},l} e^{i\mathbf{k}\cdot\mathbf{r}} \phi_{l,s}(\mathbf{k}) c_{l,s}(\mathbf{k}) \delta_{\tau,\tau_l}. \quad (16)$$

The single-particle states appearing in this expression are the HF wave functions, Eq. (13). We do not consider intervalley particle-hole operators as this would involve large momentum imparted to the system. Assuming translational invariance, in momentum space the response function has the form

$$\chi_\tau(\mathbf{q}, t) = -\frac{i\Theta(t)}{L_x L_y} \sum_{\{\mathbf{k}_i, \mathbf{q}_i, l_i\}} f_{l_1 l_2, \uparrow\downarrow}(\mathbf{k}_1 + \mathbf{q}, \mathbf{k}_1) f_{l_3 l_4, \downarrow\uparrow}(\mathbf{k}_2 - \mathbf{q}, \mathbf{k}_2) \langle [e^{iHt} c_{l_1\uparrow}^\dagger(\mathbf{k}_1 + \mathbf{q}) c_{l_2\downarrow}(\mathbf{k}_1) e^{-iHt}, c_{l_3\downarrow}^\dagger(\mathbf{k}_2 - \mathbf{q}) c_{l_4\uparrow}(\mathbf{k}_2)] \rangle$$

$$\equiv \frac{1}{L_x L_y} \sum_{\{\mathbf{k}_i, \mathbf{q}_i, l_i\}} f_{l_1 l_2, \uparrow\downarrow}(\mathbf{k}_1 + \mathbf{q}, \mathbf{k}_1) f_{l_3 l_4, \downarrow\uparrow}(\mathbf{k}_2 - \mathbf{q}, \mathbf{k}_2) \tilde{\chi}_{l_1 l_2 l_3 l_4}(\mathbf{k}_1, \mathbf{k}_2, \mathbf{q}, t), \quad (17)$$

with

$$\tilde{\chi}_{l_1 l_2 l_3 l_4}(\mathbf{k}_1, \mathbf{k}_2, \mathbf{q}, t) = -i\Theta(t) \langle [e^{iHt} c_{l_1\uparrow}^\dagger(\mathbf{k}_1 + \mathbf{q}) c_{l_2\downarrow}(\mathbf{k}_1) e^{-iHt}, c_{l_3\downarrow}^\dagger(\mathbf{k}_2 - \mathbf{q}) c_{l_4\uparrow}(\mathbf{k}_2)] \rangle. \quad (18)$$

It is implicit that the τ_l content of each l index on the right-hand side of this equation is a single value of τ, and the Hamiltonian appearing in the $e^{\pm iHt}$ factors is $H = H_0 + H_{\text{int}}$, using Eqs. (1) and (8). The weights $f_{l_i l_j, \sigma\sigma'}(\mathbf{k}_1, \mathbf{k}_2) \equiv \phi_{l_i,\sigma}^\dagger(\mathbf{k}_1) \phi_{l_j,\sigma'}(\mathbf{k}_2)$ are wave function overlap factors, and the indices l_i have allowed values $\tau_l = \pm 1$ and $\alpha_l = \pm 1$. To obtain an explicit expression for $\tilde{\chi}$, we take a time derivative of its definition implicit in Eq. (17), which generates expectation values involving two-, four-, and six-fermion operators. We approximate the last of these using a HF decomposition [12], leading to a closed expression for the response function that involves elements of the static density matrix described in the last section. This is the form in which we

carry out the time-dependent Hartree-Fock approximation. The resulting equation may be expressed as

$$i\partial_t \tilde{\chi}_{l_1l_2l_3l_4}(\mathbf{k}_1,\mathbf{k}_2,\mathbf{q},t) = \{n_{l_1\uparrow}(\mathbf{k}_1+\mathbf{q}) - n_{l_2\downarrow}(\mathbf{k}_1)\}\delta_{l_1l_4}\delta_{l_2l_3}\delta_{\mathbf{k}_1,\mathbf{k}_2-\mathbf{q}} - [\tilde{\epsilon}_{l_1,\uparrow}(\mathbf{k}_1+\mathbf{q}) - \tilde{\epsilon}_{l_2,\downarrow}(\mathbf{k}_1)]\tilde{\chi}_{l_1l_2l_3l_4}(\mathbf{k}_1,\mathbf{k}_2,\mathbf{q},t)$$

$$+ 2U\sum_{ab}\{\phi^a_{l_1\uparrow}(\mathbf{k}_1+\mathbf{q})[n_{l_2\downarrow}(\mathbf{k}_1) - n_{l_1\uparrow}(\mathbf{k}_1+\mathbf{q})]\phi^{b*}_{l_2\downarrow}(\mathbf{k}_1)\}\tilde{\chi}^{ab}_{\uparrow\downarrow l_3l_4}(\mathbf{k}_1,\mathbf{k}_2,\mathbf{q},t), \qquad (19)$$

where

$$\tilde{\chi}^{ab}_{s_1s_2l_3l_4}(\mathbf{k}_2,\mathbf{q},t) \equiv \sum_{l_1l_2\mathbf{k}_1}\phi^{a*}_{l_1s_1}(\mathbf{k}_1+\mathbf{q})\phi^b_{l_2s_2}(\mathbf{k}_1)\tilde{\chi}_{l_1l_2l_3l_4}(\mathbf{k}_1,\mathbf{k}_2,\mathbf{q},t)$$

defines $\tilde{\chi}^{ab}_{\uparrow\downarrow l_3l_4}$ and $\phi^a_{l,s}$ is the amplitude for the ath orbital [see Eq. (13)]. Some details leading up to Eq. (19) are provided in Appendix A. Fourier transforming Eq. (19) with respect to time, with further work it may be cast in the form

$$-\chi^{cd,c'd'}_0(\mathbf{q},\omega) = \chi^{cd,c'd'}(\mathbf{q},\omega) - 2U_0\sum_{ab}\chi^{cd,ab}_0(\mathbf{q},\omega)\chi^{ab,c'd'}(\mathbf{q},\omega). \qquad (20)$$

Here $U_0 = L_xL_yU$, $\chi^{cd,c'd'}(\mathbf{q},\omega) \equiv \frac{1}{L_xL_y}\sum_{l_3,l_4,\mathbf{k}}\tilde{\chi}^{cd}_{\uparrow\downarrow l_3l_4}(\mathbf{k},\mathbf{q},\omega)\phi^{c'}_{l_4\uparrow}(\mathbf{k})\phi^{d'*}_{l_3\downarrow}(\mathbf{k}-\mathbf{q})$, and

$$\chi^{ab,cd}_0(\mathbf{q},\omega) = -\frac{1}{L_xL_y}\sum_{l_3,l_4,\mathbf{k}_2}\frac{n_{l_4\uparrow}(\mathbf{k}_2) - n_{l_3\downarrow}(\mathbf{k}_2-\mathbf{q})}{\omega + i\delta + \tilde{\epsilon}_{l_4,\uparrow}(\mathbf{k}_2) - \tilde{\epsilon}_{l_3,\downarrow}(\mathbf{k}_2-\mathbf{q})}\phi^{a*}_{l_4\uparrow}(\mathbf{k}_2)\phi^b_{l_3\downarrow}(\mathbf{k}_2-\mathbf{q})\phi^c_{l_4\uparrow}(\mathbf{k}_2)\phi^{d*}_{l_3\downarrow}(\mathbf{k}_2-\mathbf{q}) \qquad (21)$$

is the susceptibility associated with the single-particle Hamiltonian $H^{0,HF}$, which may be viewed as a 4×4 matrix written in the basis AA, BB, AB, BA.

Finally, we write Eq. (20) in matrix form and relate it to the physical response function in Eq. (17), yielding

$$\chi_\tau(\mathbf{q},\omega) = -\mathrm{Tr}'\{[1 - 2U_0\chi_0(\mathbf{q},\omega)]^{-1}\chi_0(\mathbf{q},\omega)\}. \qquad (22)$$

In this equation, all the matrices are 4×4, but the Tr' is taken only over the "diagonal" elements, $\mathrm{Tr}'\chi^{ab,cd} = \sum_{a,c=A,B}\chi^{aa,cc}$. Equation (22) is one of our main results.

When $\mathrm{Im}\chi(\mathbf{q},\omega) \neq 0$, the system may absorb energy from a perturbation that flips an electron spin, so that the system has spin excitations with energy ω at momentum q; as a function of ω for fixed q, this comes either over a range of frequencies, where there is a continuum of excitations, or as sharp poles where there is a collective mode [12]. The latter case is characterized by $\mathrm{Det}[1 - 2U_0\chi_0(\mathbf{q},\omega)] = 0$. An example of $\chi(\mathbf{q},\omega)$ is illustrated in Fig. 1, where both a continuum and a sharp collective mode are evident. Figure 4 shows the same example on a linear scale. In this case a sharp collective mode is expected at the point where the relevant determinant vanishes. This mode is separated from the "incoherent" particle-hole excitations whose edge is denoted by ω_c.

In addition to the collective mode that is evident in Fig. 4, a second mode arises very close to the particle-hole continuum edge, which is rather difficult to discern in the response function due to its close proximity to the continuum excitations. The presence of such a mode can be demonstrated explicitly by examining the low-hole-doping limit. We now turn to this discussion.

V. SPIN-WAVE MODES FOR SMALL HOLE DOPING

For small densities of holes, it is possible to make analytical progress on finding zeros of $\mathrm{Det}[1 - 2U\chi_0(\mathbf{q},\omega)]$ in the limit $q \to 0$, indicating the location of sharp, collective spin-wave modes. Specifying $\tau = 1$ as the valley we will focus upon, the valence bands are indexed by $\alpha = -1$ in Eq. (14).

The dominant contributions to χ_0 in Eq. (21) come from $l_3 = l_4 = \{\tau = 1, \alpha = -1\}$. This leads to the approximate expression

$$\tilde{\chi}^{ab,cd}_0(\mathbf{q}=0) = -\frac{1}{L_xL_y}\sum_{\mathbf{k}}M^{ab,cd}(\mathbf{k})\frac{\Delta n(k)}{\omega + i\delta + \Delta\tilde{\epsilon}(k)}, \qquad (23)$$

where $\Delta n(k) = n_\uparrow(k) - n_\downarrow(k)$ and $\Delta\tilde{\epsilon}(k) = \lambda - (\tilde{m}_\uparrow - \tilde{m}_\downarrow) - U[n_\uparrow(k) - n_\downarrow(k)] - \frac{1}{2}(\frac{1}{\tilde{m}_\uparrow} - \frac{1}{\tilde{m}_\downarrow})(atk)^2 \equiv E_0 - \frac{1}{2}\gamma k^2$, where $E_0 = \lambda - (\tilde{m}_\uparrow - \tilde{m}_\downarrow) - U_0[n_\uparrow(k) - n_\downarrow(k)]$ and $\gamma = (\frac{1}{\tilde{m}_\uparrow} - \frac{1}{\tilde{m}_\downarrow})(at)^2$. Notice we have employed a small k expansion of $\tilde{\epsilon}(k)$, which works well because $\Delta n(k)$ differs from zero only at small k in the low-hole-doping limit.
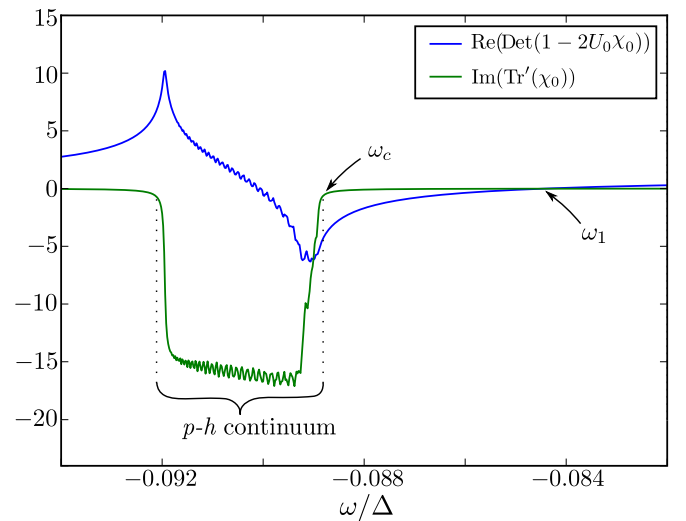

FIG. 4. Plot of a typical $\chi(\mathbf{q},\omega)$, Eq. (22), showing the particle-hole excitations of the spin-split valence bands below an energy ω_c. At ω_1, there is a single collective mode visible for which the real part of the denominator of Eq. (22) is zero. Here we have used $\mathbf{q} = \mathbf{0}$, $\mu_0 = -0.49\Delta$, $\tau = +1$, and $U_0 = 0.2$eV.

The particle-hole continuum is identified by the interval of ω for which $\omega + \Delta\tilde{\epsilon}(k)$ vanishes for some k where $\Delta n(k) \neq 0$. This range is given in the present approximation by $-E_0 < \omega < -E_0 + \frac{1}{2}\gamma k_F^2 \equiv \omega_c$, where k_F is the Fermi wave vector for the pocket of holes in the valence band.

The matrix elements $M^{ab,cd}(\mathbf{k}) = \phi_\uparrow^{a*}(\mathbf{k})\phi_\downarrow^b(\mathbf{k})$ can be obtained by similarly expanding the Hartree-Fock wave functions for small k,

$$\tilde{\phi}_s(\mathbf{k}) \approx \begin{bmatrix} e^{-i\phi}\frac{atk}{2\tilde{m}_s} \\ -\left[1 - \frac{(atk)^2}{8\tilde{m}_s^2}\right] \end{bmatrix}, \qquad (24)$$

where only up to second-order terms in k are kept. To this order the only relevant nonvanishing elements of the M matrix are

$$M^{AA,BB} = M^{BB,AA} = \frac{(atk)^2}{4\tilde{m}_\uparrow \tilde{m}_\downarrow},$$

$$M^{BB,BB} = 1 - \frac{(atk)^2}{4\tilde{m}_\uparrow^2} - \frac{(atk)^2}{4\tilde{m}_\downarrow^2},$$

$$M^{AB,BA} = M^{BA,AB} = \frac{(atk)^2}{4\tilde{m}_\uparrow^2}.$$

Except for $M^{AA,AA}$, which vanishes to $O(k^2)$, all the other entries of M contain phases of the form $e^{-i\phi}$, with ϕ being the angle of $\mathbf{k}$ with respect to the k_x axis, which vanishes upon integration over momentum. Thus these do not contribute to $\tilde{\chi}_0$. At $\mathbf{q} = 0$, $\tilde{\chi}_0$ has a block-diagonal form, and $\mathrm{Det}[1 - 2U\chi_0(\mathbf{q}, \omega)]$ can be written as the product of two subdeterminants, D_1 and D_2, given by

$$D_1 = \left(1 - 2U_0\tilde{\chi}_0^{AA,AA}\right)\left(1 - 2U_0\tilde{\chi}_0^{BB,BB}\right) - 4U_0^2 \tilde{\chi}_0^{AA,BB}\tilde{\chi}_0^{BB,AA}, \qquad (25)$$

$$D_2 = 1 - 4U_0^2 \tilde{\chi}_0^{AB,BA}\tilde{\chi}_0^{BA,AB}. \qquad (26)$$

If either of these vanishes at an ω outside the particle-hole continuum frequency interval, there is a sharp collective mode at that frequency. Note that particular response functions appearing in D_1 and D_2 indicate that the former is associated with spin flips in which electrons remain in the same orbital, while the latter arises due to electrons which both flip spin and change orbital.

Using the integrals

$$I_0 = \frac{1}{L_x L_y}\sum_{|\mathbf{k}|<k_F}\frac{1}{\omega + E_0 - \frac{1}{2}\gamma k^2}$$

$$= \int_0^{k_F}\frac{k\,dk}{2\pi}\frac{1}{\omega + E_0 - \frac{1}{2}\gamma k^2}$$

$$= -\frac{1}{2\pi\gamma}\ln\left(\frac{\omega + E_0 - \frac{1}{2}\gamma k_F^2}{\omega + E_0}\right) \qquad (27)$$

and

$$I_1 = \frac{1}{L_x L_y}\sum_{|\mathbf{k}|<k_F}\frac{k^2}{\omega + E_0 - \frac{1}{2}\gamma k^2}$$

$$= \frac{1}{2\pi\gamma}\left[-\frac{\omega + E_0}{\gamma}\ln\left(\frac{\omega + E_0 - \frac{1}{2}\gamma k_F^2}{\omega + E_0}\right) - k_F^2\right], \qquad (28)$$

the condition $D_1 = 0$ reduces to

$$1 - 2U_0\left[I_0 - \frac{(at)^2}{4}\left(\frac{1}{\tilde{m}_\uparrow^2} + \frac{1}{\tilde{m}_\downarrow^2}\right)I_1\right] = \frac{U_0^2(at)^4}{4\tilde{m}_\uparrow^2 \tilde{m}_\downarrow^2}. \qquad (29)$$

Similarly, $D_2 = 0$ can be simplified to

$$I_1 = \pm\frac{2\tilde{m}_\uparrow \tilde{m}_\downarrow}{U_0(at)^2}. \qquad (30)$$

The condition (29) will be met for some value of ω outside the particle-hole continuum for small interaction strength U_0. This can be understood as follows. For small U_0, we approximate the equation as

$$\frac{(at)^2}{4}\left(\frac{1}{\tilde{m}_\uparrow^2} + \frac{1}{\tilde{m}_\downarrow^2}\right)I_1 \approx I_0 - \frac{1}{2U_0}. \qquad (31)$$

Using the fact that

$$I_1 = \frac{\omega + E_0}{\gamma}I_0 - \frac{k_F^2}{2\pi\gamma},$$

this equation can be recast as

$$I_0 = \frac{(at/2)^2\left(\frac{1}{\tilde{m}_\uparrow^2} + \frac{1}{\tilde{m}_\downarrow^2}\right)\frac{k_F^2}{2\pi\gamma} - \frac{1}{2U_0}}{(at/2)^2\left(\frac{1}{\tilde{m}_\uparrow^2} + \frac{1}{\tilde{m}_\downarrow^2}\right)\frac{E_0+\omega}{\gamma} - 1}. \qquad (32)$$

The numerator of the right-hand side of this equation is negative for small U_0. As ω increases from large negative values, the right-hand side is positive and increases in magnitude, diverging at

$$\omega = \omega_{\text{div}} \equiv -E_0 + \frac{4\gamma}{a^2t^2}\left(\frac{1}{\tilde{m}_\uparrow^2} + \frac{1}{\tilde{m}_\downarrow^2}\right)^{-1}. \qquad (33)$$

Importantly, $\omega_{\text{div}} > \omega_c$ in the low-doping limit, so the divergence is above the particle-hole continuum. Above ω_{div} the right-hand side increases uniformly from arbitrarily large negative values, eventually vanishing at large positive ω. By contrast, I_0 diverges to large negative values as $\omega \to -E_0$ from below and comes down from arbitrarily large positive values starting at the particle-hole continuum edge ω_c. This guarantees there will be a crossing of the left- and right-hand sides of Eq. (32) between this edge and ω_{div} and a collective mode with frequency ω_1 in this interval. This is qualitatively shown in Fig. 5. Note that for decreasing U_0 this solution moves closer to the particle-hole continuum, which we indeed find numerically, as illustrated in Fig. 6. As is shown in Appendix B, for small U_0 and small hole doping, one can show that for $\mathbf{q} = 0$

$$\omega_1 \approx -E_0 + \frac{1}{2}\gamma k_F^2(1 + e^{-\pi\gamma/U_0}). \qquad (34)$$

The second condition (30), for small U_0, can be satisfied only for the negative sign of the right-hand side. The position of the spin-wave mode at $\mathbf{q} = 0$ can be approximately evaluated to be

$$\omega_2 \approx -E_0 + \frac{1}{2}\gamma k_F^2(1 + e^{-\epsilon_0/k_F^2 U_0}), \qquad (35)$$

where $\epsilon_0 = 8\pi\tilde{m}_\uparrow\tilde{m}_\downarrow/a^2t^2$. It is clear from Eqs. (34) and (35) that the separation of ω_2 from the particle-hole continuum
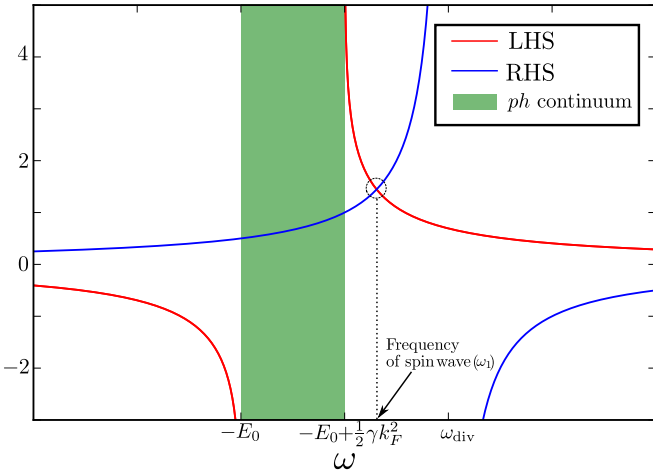
FIG. 5. Schematic representation of the left- and right-hand sides of Eq. (32) as functions of ω, shown in red and blue, respectively. For low enough k_F, an isolated spin-wave mode is always present.

is very small when compared to that of ω_1 for small hole doping and for the relevant parameter range. This result is again consistent with our numerical solutions, as illustrated in Fig. 6.

We conclude this section with two comments on these results. First, the appearance of a sharp collective mode with arbitrarily small U_0 supports the interpretation of the noninteracting ground state as being effectively polarized in a "pseudospin" spin variable, $\sigma_z \tau_z$, as discussed in the Introduction. When interactions are introduced, incoherent particle-hole excitations are pushed up in energy via a loss of exchange energy which, for repulsive interactions, generically lowers the ground-state energy for a polarized state. However, an appropriate linear combination of particle-hole pair states can minimize this loss of exchange energy, leading to the sharp collective mode.

Second, although we have demonstrated the existence of two discrete modes, the second of these (at $\omega = \omega_2$) lies exceedingly close to the particle-hole continuum edge. This means that small perturbations can easily admix these different kinds of modes together, making the detection of the second mode challenging. Indeed, in our own numerics the

introduction of broadening in our discrete wave vector sum, introduced to simulate the thermodynamic limit, typically mixes this mode with the continuum. In this situation the mode does not show up sharply in the response function we focus upon. We note that our analysis shows the mode to be associated with simultaneous spin flip *and* a change of orbital, $A \leftrightarrow B$, so that we expect this second mode should show up more prominently in more complicated response functions that simultaneously probe both of these.

VI. NUMERICAL RESULTS AND DISCUSSION

In general, to compute χ_τ we need to know χ_0. This can be obtained numerically, and we accomplish this by approximating the integral in Eq. (21) as a discrete sum. For our calculations we discretize momenta onto a 100×100 two-dimensional grid, with each momentum component running from $-k_0$ to $+k_0$. We have checked that the contribution to χ_0 dies off quickly within the range of momentum integration. We also discretize ω to a set of 5000 points, within which we compute physical response functions. A small but nonvanishing imaginary η is retained, of the order of the spacing of the ω values, to produce the continuity expected in the thermodynamic limit (where the momentum grid over which we sum becomes arbitrarily fine). Figures 1 and 4 depict typical results.

The response function (15) qualitatively describes the dynamics of an electron-hole pair between bands of opposite spins. The lowest-energy excitations necessarily involve the bands nearest the chemical potential μ. When μ is within the gap so that the system is insulating, such an excitation will have energy comparable to the band gap $E_g \sim 1$ eV [16–18]. On the other hand, when hole doped, the chemical potential falls below the top of the valence band; electron-hole pairs from the two spin species in the valence band become available (see Fig. 3). The resulting excitations can have energy of order $\lambda \sim 0.1$ eV, a considerably lower energy scale. Discrete poles in χ have infinite lifetime and represent the collective spin-wave modes of the system; these can arise only when interactions are included in the model. A set of representative plots illustrating both the spin-wave dispersion and the particle-hole continuum is shown in Fig. 7 for both the valleys. Note the clear symmetry apparent between the two
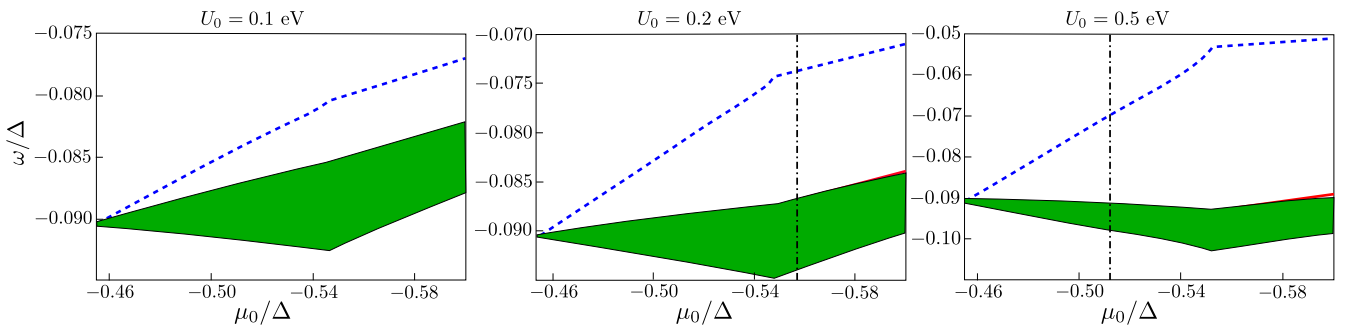

FIG. 6. Spin-wave excitations and the particle-hole continuum as a function of the chemical potential μ_0 shown for three different values of the interaction strength U_0 when $\mathbf{q} = \mathbf{0}$. The green band corresponds to the particle-hole continuum, as shown in Fig. 4. The blue dashed line corresponds to the isolated mode at frequency ω_1 described in Figs. 4 and 5. The mode corresponding to Eq. (35) is barely visible as a red line. The vertical lines indicate the boundary beyond which the stability condition is violated (see main text for details).
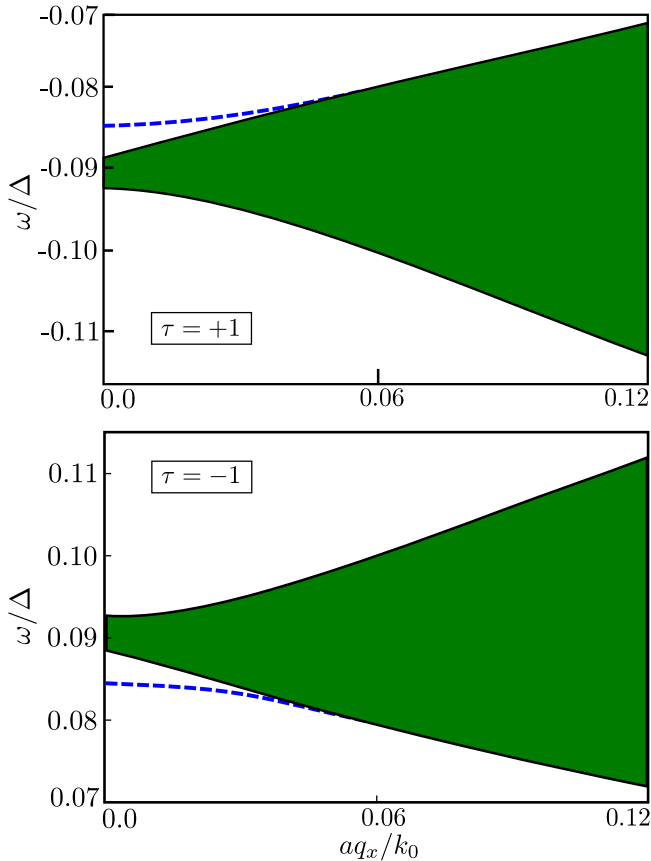
FIG. 7. The blue line depicts the dispersion of the isolated spin-wave excitation, i.e., the ω, q_x points for which the real part of the denominator of the spin susceptibility given by Eq. (22) vanishes. The green continuum represents the particle-hole excitations for which the denominator of Eq. (22) has a nonvanishing imaginary component, as shown in Fig. 4. Here we have taken $U_0 = 0.2$ eV.

valley responses when $\omega \to -\omega$. This is a manifestation of time-reversal symmetry and indicates that strong absorption from a perturbation with one helicity in one of the two valleys implies equally strong absorption in the other valley when the helicity is reversed.

It is interesting to consider the possible consequences of this if the system develops true ferromagnetism, which is thought to occur above some critical interaction strength U_c [10,11]. In the simplest description, this leads to different self-consistent exchange fields and different hole populations for each valley [11]. The computation of spin response in this situation is essentially the same as carried out in our study, but the effective chemical potential would be different for each valley. In this case we expect the spin response to be different for the two possible perturbations, reflecting the broken time-reversal symmetry in the ground state. Such behavior has indeed been observed for *electron*-doped TMDs [10].

Another feature apparent in Fig. 6 is a cusp in the continuum spectrum, which appears at $\mu_0 = \mu_c \approx -0.55\Delta$. This is the point at which the chemical potential touches the top of the lower valence band (Fig. 3). For $\mu_0 > \mu_c$, a particle-hole continuum is present only at nonvanishing frequencies

determined by the difference in energy between the highest occupied and lowest unoccupied bands of opposite spins. However, for $\mu_0 \lesssim \mu_c$, low-energy particle-hole excitations set in for processes in which (for one of the valleys) a spin-down valence band electron is excited to the spin-up valence band at finite wave vector but vanishing frequencies. This is further illustrated in Fig. 2, in which one finds the continuum excitations reaching down to zero energy, at a finite q_x, only when the chemical potential is below this critical value.

As is apparent from Fig. 4, the first spin-wave mode from the condition (32) appears above the continuum. Further, for a given U_0, the separation from the continuum increases linearly with increasing hole doping, as illustrated in Fig. 7, until the chemical potential touches the top of the lower valence band. At this point a cusp similar to that for the continuum appears in the spin-wave dispersion. The linear increase of the separation between the spin-wave mode and the top of the particle-hole continuum at small hole doping can be understood in the following way. As shown in Appendix B, Eq. (32) can be approximated for small hole doping and small U_0 by

$$\frac{\delta_0}{\delta_0 + c_0 \delta\mu} \approx e^{-\pi\gamma/U}, \tag{36}$$

where δ_0 is the separation of the spin wave from the continuum and $\delta\mu$ is the change in chemical potential due to hole doping and the constant $c_0 = \gamma/\tilde{m}_\uparrow$. As the right-hand side of the equation is independent of $\delta\mu$, the solution δ_0 should also be proportional to $\delta\mu$.

As discussed in the previous section, the second spin-wave solution of Eq. (35) lies extremely close to the continuum and so is almost invisible in our numerical solutions for the range of the parameters we consider. One expects this mode to be visible for larger U_0 and larger hole doping. However, in our calculations we find that the stability condition [12] $\omega(-\text{Im}\chi_\tau) > 0$ fails for some range of ω for U_0 large enough that we are able to numerically resolve the mode from the continuum. An example of this is shown in Fig. 8. The point beyond which this stability condition is not satisfied is indicated by vertical lines in Fig. 6. Note that, physically, the instability we find in the response functions indicates that the symmetry of the ground state we are assuming is broken, very likely into a state with interorbital coherence. Whether such a state exists at large U or is preempted by a first-order transition into a state with different hole populations in the valleys requires a more general Hartree-Fock study than we have presented in this work and is left for future study.

VII. SUMMARY

In this paper, we have studied collective excitations of a simple TMD model, showing that even without the formation of spontaneous magnetic order, interactions induce sharp collective modes that are commonly associated with such order. The presence of these modes can be understood as a consequence of intrinsic order induced by the strong spin-orbit interaction that yields different energetic orderings of spins in different valleys and arises when the system is doped. The presence of these modes is a direct analog of Silin-Leggett modes present in a simple Fermi liquid subject
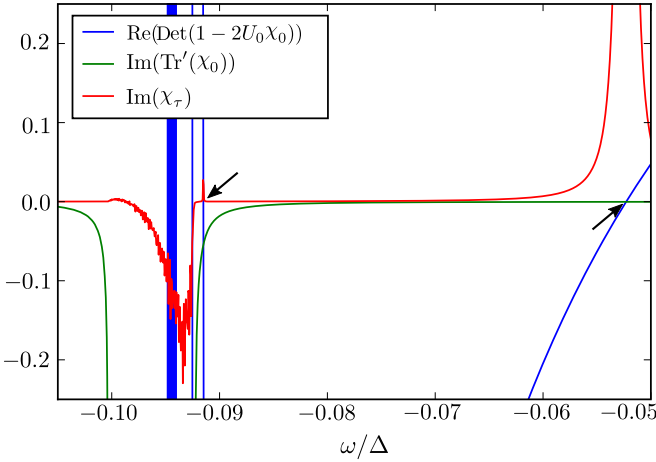
FIG. 8. Spin susceptibility for $U_0 = 0.5$ eV, $\tau = +1$, and $\mu_0 = -0.57\Delta$. Two discrete spin-wave modes (indicated by arrows) are visible near $\omega = -0.055\Delta$ and $\omega = -0.092\Delta$, with the second mode very close to the continuum. However, the positivity $\omega(-\mathrm{Im}\chi) > 0$ does not hold for all ω, implying that our assumed Hartree-Fock state is not the true ground state.

to a magnetic field, such that the Fermi wave vector becomes spin dependent. Our analysis is developed using the time-dependent Hartree-Fock approximation of a physical spin response function and reveals two sharp modes in addition to a continuum of particle-hole excitations. While one of these modes (associated with spin flips for electrons maintaining their orbital index) breaks out from the continuum in a clear way, the other (associated with electrons changing both spin and orbital) remains very close to the continuum edge and is difficult to distinguish independently. Signatures of how the subbands are populated can be seen in properties of the spin response functions when the chemical potential is modified, which, in principle, can be accomplished by gating the system.

Our calculations indicate that with strong enough interaction the system becomes unstable. Within our model this would likely be to a state with interorbital coherence, but first-order instabilities in which the system spontaneously forms unequal valley and spin populations are also possible, which may preempt any instability indicated in linear response. The validity of the simple model that we use, Eq. (1), is also limited by the positions of other bands in the system, notably, at the Γ point [4]. For MoS_2, this separation is small as bands near the Γ point lie 0.1–0.2 eV below the tops of the bands at the K, K' points. The separation in energy is larger for certain dichalcogenides, such as WS_2, $MoSe_2$, WSe_2, $MoTe_2$, and WTe_2, among others. Our results, which are based on a simple two-band model near the K, K' points, will change qualitatively when the Fermi energy is low enough that bands at the Γ points contain holes. Whatever the true ground state of the system, our formalism, in principle, allows a calculation of the density matrix associated with it and of collective modes around it. Moreover, the approach we present can be extended to more general response functions (for example, involving the spin and orbital simultaneously) which could reveal further and perhaps clearer signatures of the two collective modes we find in our analysis. Exploration of these represents interesting directions for future work.

APPENDIX A: DETAILS OF TIME-DEPENDENT HARTREE-FOCK APPROXIMATION

In this appendix we provide a few details of the calculation leading to Eq. (19). The equation of motion of $\tilde{\chi}$, Eq. (18), is

$$i\partial_t \tilde{\chi}_{l_1 l_2 l_3 l_4}(\mathbf{k}_1 \mathbf{k}_2 \mathbf{q}, t) = \{n_{l_1\uparrow}(\mathbf{k}_1 + \mathbf{q}) - n_{l_2\downarrow}(\mathbf{k}_1)\}\delta_{l_1 l_4}\delta_{l_2 l_3}\delta_{\mathbf{k}_1, \mathbf{k}_2 - \mathbf{q}} + i\Theta(t)\langle\{[H_0, c^\dagger_{l_1\uparrow}(\mathbf{k}_1 + \mathbf{q})c_{l_2\downarrow}(\mathbf{k}_1)](t), c^\dagger_{l_3\downarrow}(\mathbf{k}_2 - \mathbf{q})c_{l_4\uparrow}(\mathbf{k}_2)\}\rangle$$

$$+ i\Theta(t)\langle\{[H_{\text{int}}, c^\dagger_{l_1\uparrow}(\mathbf{k}_1 + \mathbf{q})c_{l_2\downarrow}(\mathbf{k}_1)](t), c^\dagger_{l_3\downarrow}(\mathbf{k}_2 - \mathbf{q})c_{l_4\uparrow}(\mathbf{k}_2)\}\rangle. \tag{A1}$$

The first commutator reads

$$[H_0, c^\dagger_{l_1\uparrow}(\mathbf{k}_1 + \mathbf{q})c_{l_2\downarrow}(\mathbf{k}_1)] = \sum_l h^0_{l l_1,\uparrow}(\mathbf{k}_1 + \mathbf{q})c^\dagger_{l\uparrow}(\mathbf{k}_1 + \mathbf{q})c_{l_2\downarrow}(\mathbf{k}_1) - \sum_{l'} h^0_{l_2 l',\downarrow}(\mathbf{k}_1)c^\dagger_{l_1\uparrow}(\mathbf{k}_1 + \mathbf{q})c_{l'\downarrow}(\mathbf{k}_1). \tag{A2}$$

The first commutator appearing in the last term of Eq. (A1) is

$$[H_{\text{int}}, c^\dagger_{l_1\uparrow}(\mathbf{k}_1 + \mathbf{q})c_{l_2\downarrow}(\mathbf{k}_1)]$$

$$= 2U \sum_{\{l_i, \mathbf{k}_i\}} \left[f_{l_6 l_7,\uparrow\uparrow}(\mathbf{k}_6, \mathbf{k}_6 + \mathbf{q}')f_{l_5 l_8,\uparrow\uparrow}(\mathbf{k}_5, \mathbf{k}_5 - \mathbf{q}')c^\dagger_{l_5\uparrow}(\mathbf{k}_5)c^\dagger_{l_6\uparrow}(\mathbf{k}_6)c_{l_7\uparrow}(\mathbf{k}_6 + \mathbf{q}')c_{l_2\downarrow}(\mathbf{k}_1)\delta_{l_1,l_8}\delta_{\mathbf{k}_5 - \mathbf{q}',\mathbf{k}_1 + \mathbf{q}} \right.$$

$$+ f_{l_6 l_7,\downarrow\downarrow}(\mathbf{k}_6, \mathbf{k}_6 + \mathbf{q}')f_{l_5 l_8,\downarrow\downarrow}(\mathbf{k}_5, \mathbf{k}_5 - \mathbf{q}')c^\dagger_{l_1\uparrow}(\mathbf{k}_1 + \mathbf{q})c^\dagger_{l_5\downarrow}(\mathbf{k}_5)c_{l_7\downarrow}(\mathbf{k}_6 + \mathbf{q}')c_{l_8\downarrow}(\mathbf{k}_5 - \mathbf{q}')\delta_{l_2,l_6}\delta_{\mathbf{k}_1,\mathbf{k}_6}$$

$$- f_{l_6 l_7,\uparrow\uparrow}(\mathbf{k}_6, \mathbf{k}_6 + \mathbf{q}')f_{l_5 l_8,\downarrow\downarrow}(\mathbf{k}_5, \mathbf{k}_5 - \mathbf{q}')c^\dagger_{l_5\downarrow}(\mathbf{k}_5)c^\dagger_{l_6\uparrow}(\mathbf{k}_6)c_{l_8\downarrow}(\mathbf{k}_5 - \mathbf{q}')c_{l_2\downarrow}(\mathbf{k}_1)\delta_{l_1,l_7}\delta_{\mathbf{k}_1 + \mathbf{q},\mathbf{k}_6 + \mathbf{q}'}$$

$$\left. - f_{l_6 l_7,\uparrow\uparrow}(\mathbf{k}_6, \mathbf{k}_6 + \mathbf{q}')f_{l_5 l_8,\downarrow\downarrow}(\mathbf{k}_5, \mathbf{k}_5 - \mathbf{q}')c^\dagger_{l_1\uparrow}(\mathbf{k}_1 + \mathbf{q})c^\dagger_{l_6\uparrow}(\mathbf{k}_6)c_{l_7\uparrow}(\mathbf{k}_6 + \mathbf{q}')c_{l_8\downarrow}(\mathbf{k}_5 - \mathbf{q}')\delta_{l_2,l_5}\delta_{\mathbf{k}_1,\mathbf{k}_6} \right]. \tag{A3}$$

Here, for notational simplicity, we have absorbed the $\delta_{\tau_i \tau_j}$ factors inside the $f_{l_i l_j}$'s. We next employ the Hartree-Fock approximation and find that the $\mathbf{q}' = 0$ terms cancel each other. The other terms are

$$\left[H_{\text{int}}, c^\dagger_{l_1 \uparrow}(\mathbf{k}_1 + \mathbf{q}) c_{l_2 \downarrow}(\mathbf{k}_1) \right]$$

$$\rightarrow -2U \sum_{\{l_i, \mathbf{k}_i\}} \left[f_{l_6 l_5, \uparrow\uparrow}(\mathbf{k}_1 + \mathbf{q}, \mathbf{k}_1 + \mathbf{q} + \mathbf{q}') f_{l_5 l_1, \uparrow\uparrow}(\mathbf{k}_1 + \mathbf{q} + \mathbf{q}', \mathbf{k}_1 + \mathbf{q}) n_{l_5 \uparrow}(\mathbf{k}_1 + \mathbf{q} + \mathbf{q}') c^\dagger_{l_6, \uparrow}(\mathbf{k}_1 + \mathbf{q}) c_{l_2, \downarrow}(\mathbf{k}_1) \right.$$

$$+ f_{l_2 l_5, \downarrow\downarrow}(\mathbf{k}_1, \mathbf{k}_1 + \mathbf{q}') f_{l_5 l_8, \downarrow\downarrow}(\mathbf{k}_1 + \mathbf{q}', \mathbf{k}_1) n_{l_5 \downarrow}(\mathbf{k}_1 + \mathbf{q}') c^\dagger_{l_1, \uparrow}(\mathbf{k}_1 + \mathbf{q}) c_{l_8, \downarrow}(\mathbf{k}_1)$$

$$- f_{l_6 l_1, \uparrow\uparrow}(\mathbf{k}_1 + \mathbf{q} - \mathbf{q}', \mathbf{k}_1 + \mathbf{q}) f_{l_2 l_8, \downarrow\downarrow}(\mathbf{k}_1, \mathbf{k}_1 - \mathbf{q}') n_{l_2 \downarrow}(\mathbf{k}_1) c^\dagger_{l_6, \uparrow}(\mathbf{k}_1 + \mathbf{q} - \mathbf{q}') c_{l_8, \downarrow}(\mathbf{k}_1 - \mathbf{q}')$$

$$+ \left. f_{l_2 l_8, \downarrow\downarrow}(\mathbf{k}_1, \mathbf{k}_1 - \mathbf{q}') f_{l_6 l_1, \uparrow\uparrow}(\mathbf{k}_1 + \mathbf{q} - \mathbf{q}', \mathbf{k}_1 + \mathbf{q}) n_{l_1 \uparrow}(\mathbf{k}_1 + \mathbf{q}) c^\dagger_{l_6, \uparrow}(\mathbf{k}_1 + \mathbf{q} - \mathbf{q}') c_{l_8, \downarrow}(\mathbf{k}_1 - \mathbf{q}') \right]. \tag{A4}$$

At this point, we would like to point out that because $f_{l_i l_j} \propto \delta_{\tau_i \tau_j}$ and $\tau_1 = \tau_2$, all the electronic operators have the same valley index τ in this expression.

Finally, we introduce $\rho^{ab}_{s_1 s_2}(\mathbf{q}) = \sum_{l l' \mathbf{k}} \phi^{a*}_{l s_1}(\mathbf{k} + \mathbf{q}) c^\dagger_{l \uparrow}(\mathbf{k} + \mathbf{q}) c_{l' \downarrow}(\mathbf{k}) \phi^b_{l s_2}(\mathbf{k})$ and $n^{ab}_s = \sum_{\mathbf{k} l} \phi^a_{l s}(\mathbf{k}) n_{l s}(\mathbf{k}) \phi^{b*}_{l s}(\mathbf{k})$ to write

$$\left[H_{\text{int}}, c^\dagger_{l_1 \uparrow}(\mathbf{k}_1 + \mathbf{q}) c_{l_2 \downarrow}(\mathbf{k}_1) \right] \rightarrow -2U \sum_{abl'} \left[n^{ab}_\uparrow \phi^b_{l_1 \uparrow}(\mathbf{k}_1 + \mathbf{q}) \phi^{a*}_{l' \uparrow}(\mathbf{k}_1 + \mathbf{q}) c^\dagger_{l' \uparrow}(\mathbf{k}_1 + \mathbf{q}) c_{l_2 \downarrow}(\mathbf{k}_1) - n^{ab}_\downarrow \phi^b_{l' \downarrow}(\mathbf{k}_1) \phi^{a*}_{l_2 \downarrow}(\mathbf{k}_1) \right.$$

$$\left. \times c^\dagger_{l_1 \uparrow}(\mathbf{k}_1 + \mathbf{q}) c_{l' \downarrow}(\mathbf{k}_1) \right] + 2U \sum_{ab} \phi^a_{l_1 \uparrow}(\mathbf{k}_1 + \mathbf{q}) \left[n_{l_1 \uparrow}(\mathbf{k}_1 + \mathbf{q}) - n_{l_2 \downarrow}(\mathbf{k}_1) \right] \phi^{b*}_{l_2 \downarrow}(\mathbf{k}_1) \rho^{ab}_{\uparrow\downarrow}(\mathbf{q}). \tag{A5}$$

Substituting Eqs. (A2) and (A5) in Eq. (A1), we obtain Eq. (19) of the main text.

APPENDIX B: SMALL HOLE DOPING

In this appendix, we supply some details underlying Eqs. (34) and (36). For small U_0, assuming that the renormalized masses $\tilde{m}_s$ are close to their noninteracting values, we can write

$$\frac{1}{\tilde{m}^2_\uparrow} + \frac{1}{\tilde{m}^2_\downarrow} \approx \left(\frac{2}{\Delta - \lambda} \right)^2 + \left(\frac{2}{\Delta + \lambda} \right)^2 \approx \frac{8}{\Delta^2}. \tag{B1}$$

Furthermore, we note

$$\frac{\gamma}{(at)^2} = \frac{1}{\tilde{m}_\uparrow} - \frac{1}{\tilde{m}_\downarrow} \approx 4 \frac{\lambda}{\Delta^2}. \tag{B2}$$

These allow Eq. (32) for small U_0 and small hole doping to be written as

$$\frac{-1}{2\pi\gamma} \ln\left(\frac{\omega - \omega_c}{\omega - \omega_c + \frac{1}{2}\gamma k^2_F} \right) \approx \frac{\frac{k^2_F}{2\pi} - \frac{\lambda}{U_0}}{\omega - \omega_c - 2\lambda + \frac{1}{2}\gamma k^2_F}, \tag{B3}$$

where $\omega_c = -E_0 + \frac{1}{2}\gamma k^2_F$ is the boundary of the continuum of particle-hole excitations. Moreover, again for small U_0, assuming the upper valence band to have spin up (which is the case for $\tau = +1$), we can write the chemical potential as $\mu_0 \approx -\frac{1}{2}\Delta + \lambda - \frac{1}{2} \frac{(at)^2 k^2_F}{m_\uparrow}$, so that the change in μ_0 due to hole doping can be written as $\delta\mu = \frac{1}{2} \frac{(at)^2 k^2_F}{m_\uparrow}$. Using this in the above equation, we get

$$\frac{-1}{2\pi\gamma} \ln\left(\frac{\omega - \omega_c}{\omega - \omega_c + c_0 \delta\mu} \right) \approx \frac{1}{2U_0}, \tag{B4}$$

where, for small $\delta\mu$, $\omega - \omega_c$ and $\frac{1}{2}\gamma k^2_F$ are neglected compared to λ. As the right-hand side is independent of $\delta\mu$, the solution $\omega - \omega_c$ should also scale as $\delta\mu$.

When U_0 is small, the above equation can be solved for $\omega = \omega_1 \approx -E_0 + \frac{1}{2}\gamma k^2_F (1 + e^{-\pi\gamma/U_0})$. Note that this result differs from that of Eq. (35) in that k^2_F appears in the exponential in the latter. This renders $|\omega_2 - \omega_c|$ much smaller than $|\omega_1 - \omega_c|$ in the low-hole-doping limit.

[1] A. H. Castro Neto, F. Guinea, N. M. R. Peres, K. S. Novoselov, and A. K. Geim, Rev. Mod. Phys. **81**, 109 (2009).

[2] K. F. Mak, C. Lee, J. Hone, J. Shan, and T. F. Heinz, Phys. Rev. Lett. **105**, 136805 (2010).

[3] A. Splendiani, L. Sun, Y. Zhang, T. Li, J. Kim, C.-Y. Chim, G. Galli, and F. Wang, Nano Lett. **10**, 1271 (2010).

[4] D. Xiao, G.-B. Liu, W. Feng, X. Xu, and W. Yao, Phys. Rev. Lett. **108**, 196802 (2012).

[5] G.-B. Liu, W.-Y. Shan, Y. Yao, W. Yao, and D. Xiao, Phys. Rev. B **88**, 085433 (2013).

[6] T. Cao, G. Wang, W. Han, H. Ye, C. Zhu, J. Shi, Q. Niu, P. Tan, E. Wang, B. Liu, and J. Feng, Nat. Commun. **3**, 887 (2012).

[7] H. Zeng, J. Dai, W. Yao, D. Xiao, and X. Cui, Nat. Nanotechnol. **7**, 490 (2012).

[8] K. Mak, K. He, J. Shan, and T. Heinz, Nat. Nanotechnol. **7**, 494 (2012).

[9] K. F. Mak, K. L. McGill, J. Park, and P. L. McEuen, Science **344**, 1489 (2014).

[10] T. Scrace, Y. Tsai, B. Barman, L. Schweidenback, A. Petrou, G. Kioseoglou, I. Ozfidan, M. Korkusinski, and P. Hawrylak, Nat. Nanotechnol. **10**, 603 (2015).

[11] J. E. H. Braz, B. Amorim, and E. V. Castro, Phys. Rev. B **98**, 161406(R) (2018).

[12] G. Giuliani and G. Vignale, *Quantum Theory of the Electron Liquid* (Cambridge University Press, Cambridge, 2005).

[13] V. Silin, Sov. Phys. JETP **6**, 945 (1958).

[14] A. Leggett, J. Phys. C **3**, 448 (1970).

[15] G. Tastevin, P. Nacher, M. Leduc, and F. Laloe, J. Phys. Lett. **46**, 249 (1985).

[16] J. S. Ross, S. Wu, H. Yu, N. J. Ghimire, A. M. Jones, G. Aivazian, J. Yan, D. G. Mandrus, D. Xiao, W. Yao, and X. Xu, Nat. Commun. **4**, 1474 (2013).

[17] M. M. Ugeda, A. J. Bradley, S.-F. Shi, F. H. da Jornada, Y. Zhang, D. Y. Qiu, W. Ruan, S. Mo, Z. Hussain, Z. Shen, F. Wang, S. G. Louie, and M. F. Crommie, Nat. Mater. **13**, 1091 (2014).

[18] F. Wu, F. Qu, and A. H. MacDonald, Phys. Rev. B **91**, 075310 (2015).

[19] M. Trushin, M. O. Goerbig, and W. Belzig, Phys. Rev. B **94**, 041301(R) (2016).

[20] A. Pinczuk, in *Perspectives in Quantum Hall Effects*, edited by S. Das Sarma and A. Pinczuk (Wiley, New York, 1997), p. 307.